Tannin-immobilized mesoporous silica bead (BT–SiO$_2$) as an effective adsorbent of Cr(III) in aqueous solutions

Xin Huang [a], Xuepin Liao [a,*], Bi Shi [b]

[a] *Department of Biomass Chemistry and Engineering, Sichuan University, Chengdu 610065, PR China*
[b] *National Engineering Laboratory for Clean Technology of Leather Manufacture, Sichuan University, Chengdu 610065, PR China*

ARTICLE INFO

ABSTRACT

This study describes a new approach for the preparation of tannin-immobilized adsorbent by using mesoporous silica bead as the supporting matrix. Bayberry tannin-immobilized mesoporous silica bead (BT–SiO$_2$) was characterized by powder X-ray diffraction to verify the crystallinity, field-emission scanning electron microscopy to observe the surface morphology, and surface area and porosity analyzer to measure the mesoporous porous structure. Subsequently, the adsorption experiments to Cr(III) were applied to evaluate the adsorption performances of BT–SiO$_2$. It was found that the adsorption of Cr(III) onto BT–SiO$_2$ was pH-dependent, and the maximum adsorption capacity was obtained in the pH range of 5.0–5.5. The adsorption capacity was 1.30 mmol g^{-1} at 303 K and pH 5.5 when the initial concentration of Cr(III) was 2.0 mmol L^{-1}. Based on proton nuclear magnetic resonance (HNMR) analyses, the adsorption mechanism of Cr(III) on BT–SiO$_2$ was proved to be a chelating interaction. The adsorption kinetic data can be well described using pseudo-first-order model and the equilibrium data can be well fitted by the Langmuir isothermal model. Importantly, no bayberry tannin was leached out during the adsorption process and BT–SiO$_2$ can simultaneously remove coexisting metal ions from aqueous solutions. In conclusion, this study provides a new strategy for the preparation of tannin-immobilized adsorbents that are highly effective in removal of heavy metals from aqueous solutions.

1. Introduction

Chromium [Cr(III)] compounds are widely used in modern industries, such as leather making, metal finishing, and petroleum refining [1,2], which inevitably results in a large quantity of Cr(III)-contaminated industrial effluents. Waters containing a high concentration of Cr(III) are extremely harmful to human beings because they are non-biodegradable in living tissues and would induce toxic and carcinogenic health effects on humans [3]. Therefore, the removal of Cr(III) from aqueous solutions arouses great attention. Many methods have been established for the removal of metal ions from aqueous solutions, such as chemical precipitation, membrane separation, electrolytic reduction, ion exchange, and adsorption [4–9]. Among these methods, adsorption is more useful and economical method for the removal of metal ions at low concentration (<100 mg L^{-1}) in aqueous solutions [10,11]. Accordingly, great effort has been put into the development of new adsorbents that are able to effectively remove Cr(III) ions from aqueous solutions [3,12,13].

More recently, tannin has emerged as a potential alternative for the removal of heavy metals from aqueous solutions [14,15]. Tannins are natural plant extracts and contain high content of multiple adjacent phenolic hydroxyls in their molecules, and thus they have strong chelating ability towards many heavy metal ions including Cr(III), Pb(II), Hg(II), Cd(II) and Au(II) [16–18]. Since tannins are water-soluble compounds, they often need to be immobilized onto water-insoluble matrixes such as agarose [19], cellulose [20], hydrotalcite [21], and collagen fiber [22]. Our previous investigation indicated that tannin-immobilized collagen fiber exhibited outstanding adsorption capacity to many metal ions [22–24]. However, in this adsorbent, a part of phenolic hydroxyls of tannins have interacted with collagen fibers through hydrogen bonds, and hence the adsorption capacity of tannins to metal ions was not fully represented. Therefore, new approaches for the immobilization of tannins should be developed to improve the adsorption capacity of tannin-immobilized adsorbents as well as its adsorption kinetics.

Silica matrix has received great attention since it shows excellent swelling resistance in different solvents and a good mechanical, thermal and chemical stability [25]. So it is possible to obtain tannin-immobilized adsorbents with excellent physical and chemical properties by using silica as a supporting matrix. On the basis of this idea, we designed a new adsorbent for the removal of Cr(III) ions by immobilizing bayberry tannin onto mesoporous silica

---

(SiO$_2$) bead. Bayberry tannin-immobilized mesoporous silica bead (BT–SiO$_2$) is expected to have fast adsorption rate and high adsorption capacity towards Cr(III) ions due to the permanent mesopore structure of SiO$_2$ bead and abundant accessible multiple adjacent phenolic hydroxyls of bayberry tannin. In this study, the adsorption behaviors of this new adsorbent to Cr(III) ions were investigated. In addition, the adsorption mechanism of BT–SiO$_2$ to Cr(III) ions was also studied using proton nuclear magnetic resonance (HNMR).

2. Materials and methods

2.1. Reagents

Bayberry tannin (BT) was obtained from the barks of *myrica esculenta* by extraction with an acetone–water solution (1:1, v/v), followed by spray drying [26]. The tannin content of the extract was 76.3% determined using hide powder method, a national standard method of China (Code: GB2615-81) [27]. Cr(NO$_3$)$_3$·6H$_2$O and all other chemicals were analytical grade reagents. The stock solution of Cr(III) (10.0 mmol L^{-1}) was prepared by dissolving Cr(NO$_3$)$_3$·6H$_2$O into deionized water, and it was diluted to an appropriate concentration when used. Diluted HNO$_3$ and NaOH solutions were used for adjusting the initial pH of solutions.

2.2. Preparation of adsorbents

2.2.1. Preparation of aminated mesoporous SiO$_2$ beads

Aminated mesoporous SiO$_2$ beads were prepared following a methodology similar to that described by Cheng et al. [28]. Briefly, 4.0 mL of cyclohexane, 1.0 mL of n-hexanol, and 1.0 mL of TritonX-100 were added into 300.0 mL deionized water under constant stirring. After 5–10 min, a fine emulsion was formed. 9.0 mL of tetraethyl orthosilicate (TEOS, silica source) and 3.0 mL of 3-aminopropyl-triethoxysilane (APES, aminating agent) were subsequently added into the emulsion and kept vigorous stirring for 12 h. Then a proper amount of ammonia (NH$_3$·H$_2$O) was dropped in so as to promote the hydrolysis of TEOS and APES. After stirring for 12 h, 2 mL of acetone, used as an emulsion breaker, was added into the emulsion, followed by vigorous stirring for another 12 h. Finally, snow-white mesoporous SiO$_2$ beads were obtained by filtration, extensively washed with deionized water, and then dried at 373 K.

2.2.2. Preparation of BT–SiO$_2$ adsorbent

1.0 g of BT was dissolved in 100 mL of deionized water and mixed with 1.0 g of aminated mesoporous SiO$_2$ beads prepared in Section 2.2.1. The mixture was stirred at 298 K for 2 h, and then 4 mL of glutaraldehyde (50%, w/w) was dropped into the mixture. Afterwards, the mixture was first stirred at 298 K for 24 h. Subsequently, brown BT–SiO$_2$ adsorbent was obtained by filtration, fully washed with deionized water and dried in vacuum at 323 K for 12 h. BT grafting degree of BT–SiO$_2$ was calculated according to the concentration difference of BT before and after the immobilization, measured by using ultraviolet visible (UV–vis). Additionally, the preparation of BT–SiO$_2$ adsorbent was repeated several times, and it showed good reproducibility.

2.2.3. Characterization of adsorbent

Specific surface area, pore size and pore size distribution of the samples were determined with surface area and porosity analyzer (TriStar 3000, Micromeritics, US) using nitrogen as the adsorption gas. Powder X-ray diffraction (XRD) spectra were obtained from X-ray diffractometer (X'pert ProMPD, Philips, Holland). Surface morphologies were examined by field-emission scanning electron microscopy (Fe-SEM, S-4800, Hitachi, Japan). The pH-dependence of the zeta potential of BT–SiO$_2$ was measured instrumentally

(Laser Zee3.0, Pen Kem Inc.) and the pH corresponding to zero point of charge (pH$_{zpc}$) of BT–SiO$_2$ was determined.

2.2.4. Adsorption experiments

2.2.4.1. Effect of initial pH on the adsorption capacity of BT–SiO$_2$ to Cr(III).
Adsorption experiments were carried out in 100 mL of 1.0 and 2.0 mmol L^{-1} Cr(III) solution, in which the adsorbent dose was 0.1 g. The pH of the solutions, ranged from 2.5 to 5.5, was adjusted using diluted HNO$_3$ solution and NaOH solution. The adsorption process was conducted at 303 K with constant stirring for 24 h. Then, the suspension was filtered and the concentration of Cr(III) in filtrate was analyzed by inductively coupled plasma atomic emission spectroscopy (ICP-AES, Optima 2100 DV, PerkinElmer, US). The adsorption capacity of Cr(III) onto BT–SiO$_2$ was calculated from the concentration difference of Cr(III) before and after the adsorption. The adsorption of Cr(III) onto commercial SiO$_2$ was also carried out as a control experiment.

2.2.4.2. HNMR studies.
In order to investigate the adsorption mechanism of BT–SiO$_2$ to Cr(III), proton nuclear magnetic resonance (HNMR) technique was employed. Considering the complexity of molecular structure of BT, pyrogallic acid was used as a model compound to simulate the interaction between BT and Cr(III). The HNMR spectrum of pyrogallic acid–Cr(III) reaction product was measured by Bruker DPX400 NMR instrument using DMSO-*d*6 as solvent. For comparison, the HNMR analysis of pyrogallic acid was also performed.

2.2.4.3. Adsorption isotherm studies.
Adsorption experiments were carried out in 100 mL of Cr(III) solution, where the initial concentrations of Cr(III) ranged from 0.1 to 4.0 mmol L^{-1} and the dose of BT–SiO$_2$ was 1.0 g L^{-1}. The pH of the solutions was 5.5 and the adsorption process was kept at 303 K for 24 h. The adsorption process was also conducted in the presence of NaNO$_3$ with concentration of 10 and 100 mmol L^{-1}, respectively. The adsorption capacity at equilibrium was calculated by the mass balance of Cr(III) before and after adsorption.

2.2.4.4. Adsorption kinetics studies.
0.1 g of BT–SiO$_2$ was suspended in 100 mL of 1.0 mmol L^{-1} Cr(III) solution. The pH of the solutions was adjusted to 5.5 and the adsorption process was conducted at 303 K with constant stirring. The concentration of Cr(III) was analyzed at a regular interval during adsorption process.

2.2.4.5. Effect of adsorbent dose on the adsorption of Cr(III).
The adsorption experiments was carried out in 100 mL of 1.0 mmol L^{-1} Cr(III) solution, in which the adsorbent dose varied from 0.01 to 0.4 g. After 2 h of adsorption, the concentration of Cr(III) in the solutions was analyzed by ICP-AES

2.2.4.6. Effect of coexisting metal ions on the adsorption of Cr(III).
Desired amounts of BT–SiO$_2$ (0.1, 0.2 and 0.3 g) was added into 100 mL mixture solution of Cr(NO$_3$)$_3$, Fe(NO$_3$)$_3$, Cu(NO$_3$)$_2$, Al(NO$_3$)$_3$, and Ca(NO$_3$)$_2$, in which the concentrations of all metal ions were 0.1 mmol L^{-1} and the initial pH of the solutions was 5.5. After 2 h of adsorption, the concentrations of Cr(III) and other metal ions in the solutions were analyzed by ICP-AES.

2.2.4.7. Stability of BT–SiO$_2$ adsorbent.
In view of practical application, the BT immobilized onto SiO$_2$ beads should be stable during the adsorption process. Thus, a precise and sensitive spectrophotometric procedure described by Butler et al. was used to quantitatively analyze the BT leaked from the adsorbent [29]. This method is based on the reduction of ferric ion to ferrous ion in the presence of tannin, followed by the formation of a ferricyanide–ferrous ion complex, called Prussian blue. The mixture
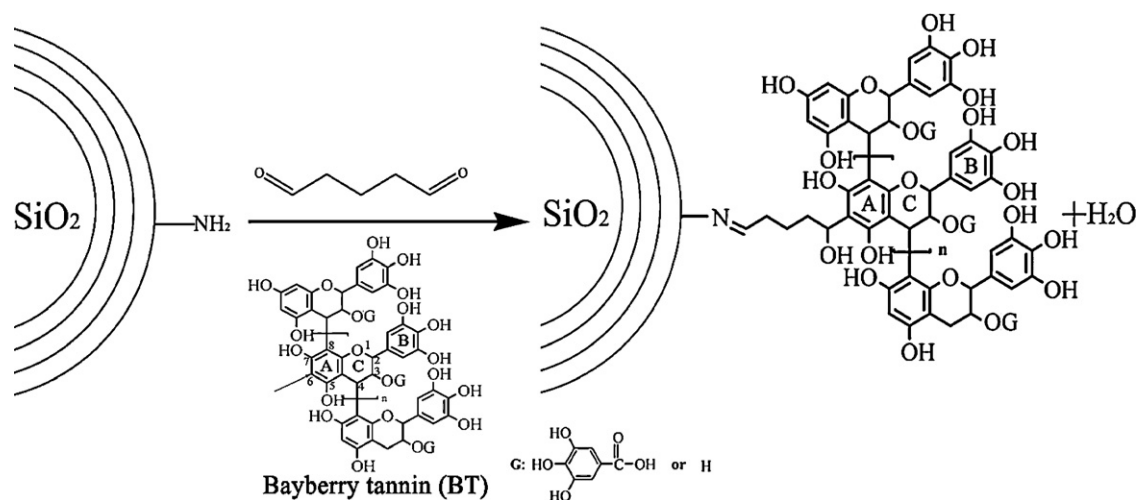
Scheme 1. The proposed synthetic routing of BT–SiO$_2$ adsorbent.

solution shows maximum absorbance at 720 nm, and therefore, the tannin content can be determined by testing the corresponding absorbance at 720 nm (A_{720}) (as shown in supporting information (SI) 1 and SI 2).

3. Results and discussion

3.1. Preparation and characterization of BT–SiO$_2$ adsorbent

As illustrated in Scheme 1, BT belongs to condensed tannin and consists of polymerized flavan-3-ols. The B rings of BT have a structure of multiple adjacent phenolic hydroxyls, which exhibit specific affinity for many metal ions via forming five-member chelate ring [30,31]. The C$_6$ of A-rings of BT has high nucleophilic reaction activity, and can form covalent bond with electrophilic agents like glutaraldehyde. In addition, glutaraldehyde is able to react with amino groups immobilized onto the surface of SiO$_2$ bead [32,31]. Thus, BT–SiO$_2$ can be prepared using glutaraldehyde as the cross-linking agent to immobilize BT onto SiO$_2$ bead, as shown in Scheme 1. The multiple adjacent phenolic hydroxyls of the B rings in BT molecules are not involved in the cross-linking reaction, which maximally retains the adsorption capacity of BT to heavy metal ions. On the other hand, many other condensed tannins, like black wattle tannin and quebracho tannin, are also suitable for preparation of tannin-immobilized SiO$_2$ bead due to their similar molecular structure and chemical properties compared with BT.

After the immobilization of BT, the snow-white color of SiO$_2$ beads was changed into dark brown, which confirmed that BT was successfully immobilized onto SiO$_2$ bead. The grafting degree of BT on BT–SiO$_2$ was 42.3% (w/w) calculated according to UV–vis measurements. The surface morphologies of BT–SiO$_2$ adsorbents were taken from Fe-SEM. As shown in Fig. 1, no precipitate of BT was observed on the surface of SiO$_2$ beads, which suggests that BT was well dispersed onto the surface of SiO$_2$ beads, and thus favors the adsorption of heavy metal ions onto BT–SiO$_2$ adsorbent. Compared with untreated SiO$_2$ bead, the XRD pattern of BT–SiO$_2$ (inserts in Fig. 1) shows the similar amorphous peak of silica at 24.4°, indicating the well preservation of SiO$_2$ structure after the immobilization of BT.

BT–SiO$_2$ adsorbent has a BET surface area of 111.12 m^2 g^{-1} and a total pore volume of 0.29 cm^3 g^{-1} based on the analysis of surface area and porosity analyzer. The N$_2$ adsorption/desorption isotherms and the pore size distribution of BT–SiO$_2$ are illustrated in Fig. 2. An obvious hysteresis loop can be observed in the adsorption/desorption isotherms of BT–SiO$_2$, indicating that the porous
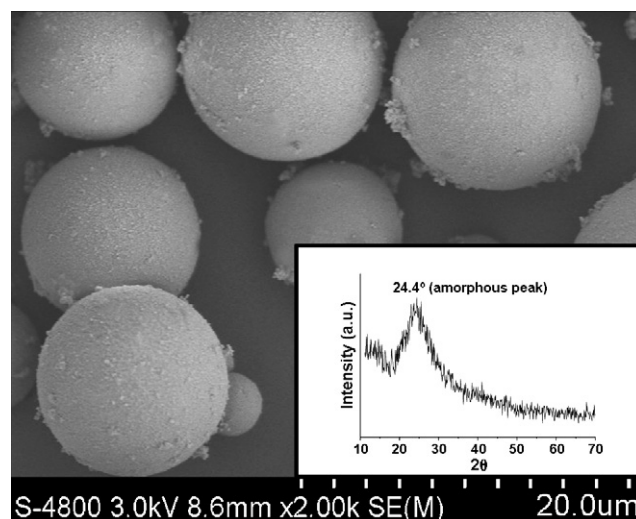

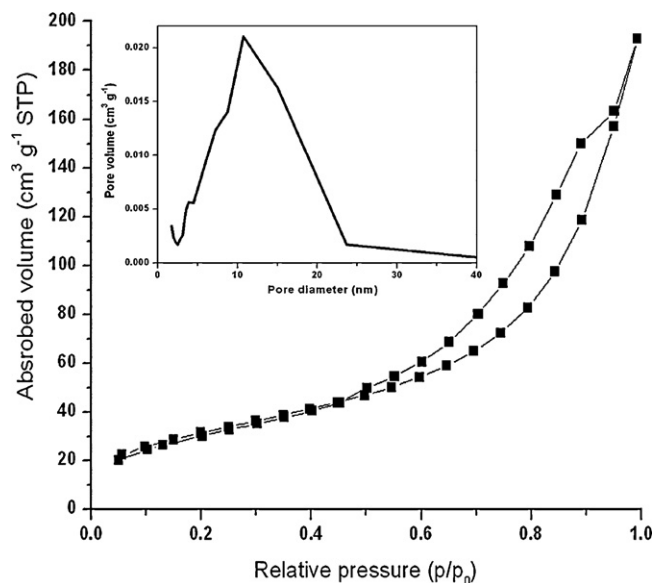**Fig. 1.** Fe-SEM images and XRD pattern (inserts) of BT–SiO$_2$ adsorbent.

Fig. 2. N$_2$ adsorption/desorption isotherms and pore size distribution plot (inserts) of BT–SiO$_2$ adsorbent.

structure of SiO_2 beads is still preserved after the immobilization of BT [33]. In addition, the pore size distribution of $BT–SiO_2$ is mainly in the range of 8.0–20.0 nm and a major peak is located at 11.0 nm (Fig. 3 inserts), which suggests that most of the pores inside the $BT–SiO_2$ adsorbent are in mesoporous structure [34,35]. It is generally accepted that mesoporous adsorbent has much higher adsorption rate compared with corresponding microporous or non-porous adsorbent, because the permanent mesoporous structure provides adsorbates an easy access to the adsorption sites, and thus decreases the mass transfer resistance during adsorption process [36,37]. From this point, a fast adsorption rate of Cr(III) onto $BT–SiO_2$ can be expected. It was found that the pH_{zpc} of $BT–SiO_2$ was pH 4.01 (as shown in SI 3).

3.2. Effect of initial pH on the adsorption of Cr(III)

The Cr(III) in aqueous solution will precipitate at $pH \geqq 6.0$ [38]. So adsorption experiments were conducted in the initial pH range of 2.5–5.5. Fig. 3 presents the effect of initial pH on the adsorption of $BT–SiO_2$ to Cr(III). Both for 1.0 and 2.0 mmol L^{-1} Cr(III) solutions, the adsorption capacity of $BT–SiO_2$ to Cr(III) slightly increased in the pH range of 2.5–4.0, and then sharply increased in the pH range of 4.0–5.5. These facts indicates that the adsorption of Cr(III) onto $BT–SiO_2$ is highly pH-dependent and is increased with the increasing pH of solution. Thermodynamic analysis indicates that Cr(III) mainly exists as Cr^{3+}, $CrOH^{2+}$ and $Cr_2(OH)_2^{4+}$ in the pH range of 2.5–5.5, as shown in Fig. 4. In the pH range of 2.5–3.9, the surface of $BT–SiO_2$ is positively charged because the solution pH is lower than the pH_{zpc} of $BT–SiO_2$. Thus, the chelating interaction of Cr(III) with phenolic hydroxyls of BT is suppressed, and the adsorption capacity is relatively lower. When the solution pH is higher than the pH_{zpc} of $BT–SiO_2$, the surface of $BT–SiO_2$ is negatively charged while more phenolic hydroxyls of BT are ionized at higher pH, which significantly promote the chelating interaction of Cr(III) with $BT–SiO_2$, resulting in the obvious increase of adsorption capacity in the range of 4.0–5.5. As the increase of initial Cr(III) concentration, the adsorption capacity of Cr(III) on $BT–SiO_2$ also increases. For example, the adsorption capacity of Cr(III) increases from 0.77 to 1.31 mol g^{-1} as the initial Cr(III) concentration increases from 1.0 to 2.0 mmol L^{-1}. This should be due to a high driving force for mass transfer at the higher initial concentration of Cr(III). Similar phenomenon was also observed by other researchers [30]. In control experiment, commercial SiO_2 had much lower adsorption capacity compared with $BT–SiO_2$ adsorbent, which confirms that the adsorption of $BT–SiO_2$
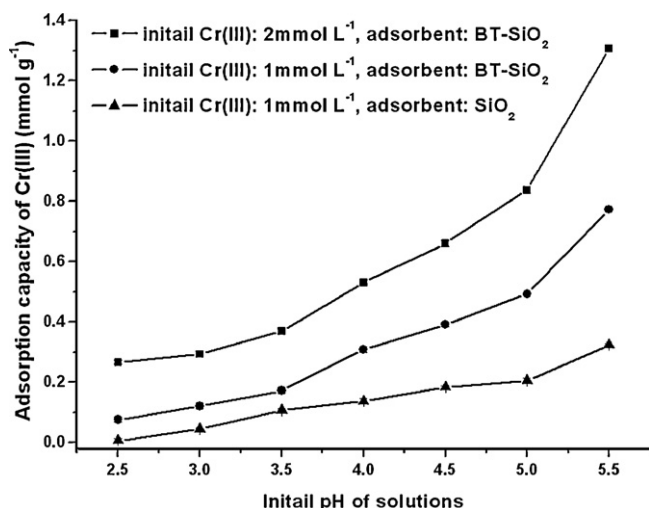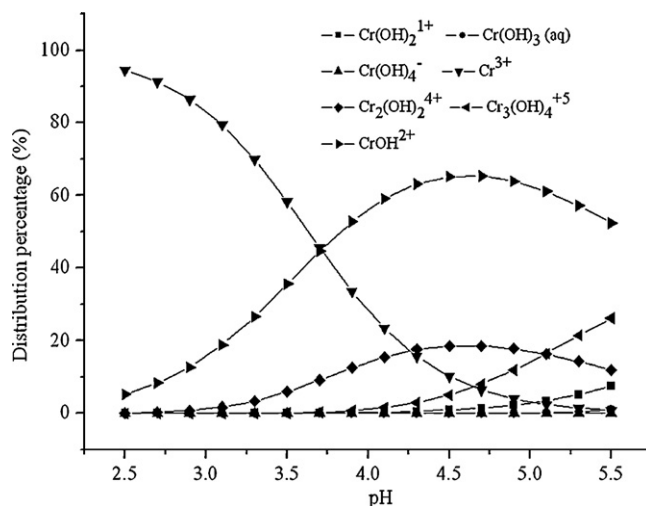

Fig. 4. Distribution of Cr(III) species in aqueous solution at different pH.(calculated by using Visual MINEQL 2.40b version, NIST database. Initial concentration of Cr(III) = 1.0 mmol L^{-1}).

to Cr(III) is mainly attributed to the immobilized BT. The maximum adsorption capacity was obtained at pH 5.5. So the following experiments were carried out in pH 5.5. In addition, $BT–SiO_2$ is stable in the pH range of 2.5–5.5 due to the fact that no solubility of SiO_2 or color change of the solution is observed during and/or after the adsorption process. In order to confirm that Cr(III) is absorbed on $BT–SiO_2$ via chelating interaction with phenolic hydroxyls of BT, pyrogallic acid was used as a model compound to stimulate the interaction between BT and Cr(III). The HNMR spectra of pyrogallic acid before and after interaction with Cr(III) are given in supporting information (SI 4). Based on the HNMR analyses, it can be concluded that $BT–SiO_2$ is able to absorb Cr(III) by chelating reaction through adjacent phenolic hydroxyls of pyrogallol structure.

3.3. Adsorption isotherm studies

Fig. 5 shows adsorption isotherms of $BT–SiO_2$ to Cr(III) at 303 K. $BT–SiO_2$ showed high adsorption capacity for Cr(III) in aqueous solutions, which is related to the large number of multiple adjacent phenolic hydroxyls of BT. For example, when the initial concen-
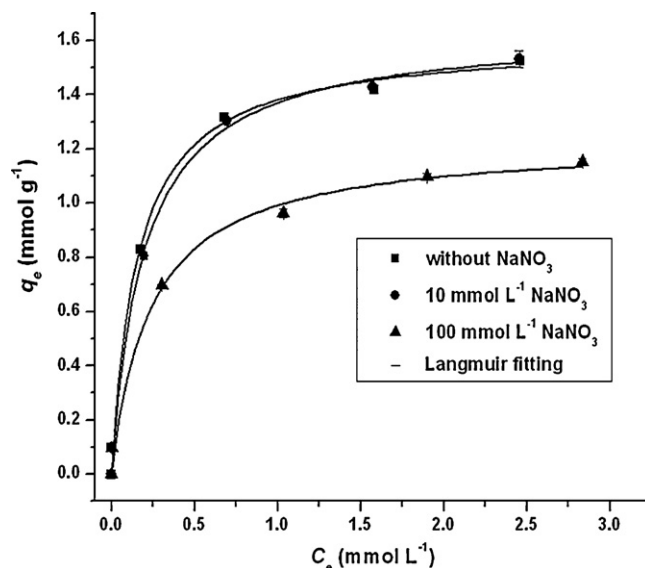

Fig. 3. The effect of initial pH on the adsorption of $BT–SiO_2$ to Cr(III).

Fig. 5. Adsorption isotherms of Cr(III) onto $BT–SiO_2$ (pH 5.5).

tration of Cr(III) was 2.0 mmol /L, the adsorption capacity of Cr(III) was high up to 1.30 mmol g^{-1}. On the other hand, the adsorption capacity of BT–SiO$_2$ to Cr(III) is almost unchanged at low concentration of NaNO$_3$ (10 mmol L^{-1}), while the effect of NaNO$_3$ cannot be neglected at higher concentration (100 mmol L^{-1}), indicating that the adsorption of Cr(III) on BT–SiO$_2$ is ionic strength dependent. Although the adsorption capacity of Cr(III) on BT–SiO$_2$ is affected at higher concentration of NaNO$_3$, it still retains at relatively high level. Strong chelating ability of BT to Cr(III) ions could be the reasonable explanation for the appreciable adsorption capacity of BT–SiO$_2$.

Adsorption isotherm data were further analyzed by the Langmuir model, which is expressed as [39]:

$$q_e = \frac{q_{max}bC_e}{1+bC_e} \tag{1}$$

where C_e is the equilibrium concentration (mmol L^{-1}), q_e is the equilibrium adsorption capacity (mmol g^{-1}), q_{max} and b are the maximum adsorption capacity (mmol/g) and the Langmuir constant relating to the strength of adsorption, respectively. The Langmuir model is based on several assumptions such as a homogeneous surface of adsorbent, a monolayer adsorption, a constant energy distribution and no interactions between adsorbed species [40]. In this study, the Langmuir model gave satisfactory fitting to the adsorption isotherm data with correlation constants higher than 0.99, indicating that Cr(III) may be adsorbed in the form of monolayer on the surface of BT–SiO$_2$.

In general, there is no theoretical model to describe the adsorption isotherms of liquid adsorption. The adsorption isotherm models used in gas adsorption are always used to describe the liquid adsorption, such as the Langmuir equation and the Freundlich equation. For gas adsorption, the monolayer coverage and/or chemical adsorption isotherms can be well described by the Langmuir model, which has strong theoretical basis. In other words, the adsorption mechanism should be monolayer coverage and/or chemical adsorption if the adsorption isotherms can be described by the Langmuir equation for a gas adsorption.

With regard to the adsorption isotherms in this research, it can be well described by the Langmuir equation. Furthermore, the chelating interaction is proved to be the mechanism of Cr(III) adsorption on BT–SiO$_2$. Thus, it is reasonable to suggest that Cr(III) is adsorbed in the form of monolayer coverage on the surface of BT–SiO$_2$.

3.4. Adsorption kinetic studies

The adsorption kinetic data are illustrated in Fig. 6. It can be seen that the adsorption rate of Cr(III) onto BT–SiO$_2$ is very fast. In the first 20 min, more than 69% of Cr(III) was adsorbed, and the adsorption equilibrium was reached at 90 min with a Cr(III) recovery percent of 77.84%. It should be noted that the adsorption rate of Cr(III) onto BT–SiO$_2$ was so fast that the adsorption capacity was high up to 0.56 mmol g^{-1} even in the first 5 min. Some other researchers also reported the fast adsorption rate of SiO$_2$-based adsorbents [41,42]. In addition to the large specific surface area of BT–SiO$_2$ (~110 m^2 g^{-1}), the fast adsorption rate of Cr(III) may be also attributed to the mesoporous structure of BT–SiO$_2$, which provides Cr(III) ion an easy access to the active sites of the adsorbent, and in turn decreases the mass transfer resistance and thus increases the adsorption efficiency. Based on the adsorption kinetic studies, all the subsequent adsorption experiments were performed for 2 h, which was considered sufficient for the removal of Cr(III).
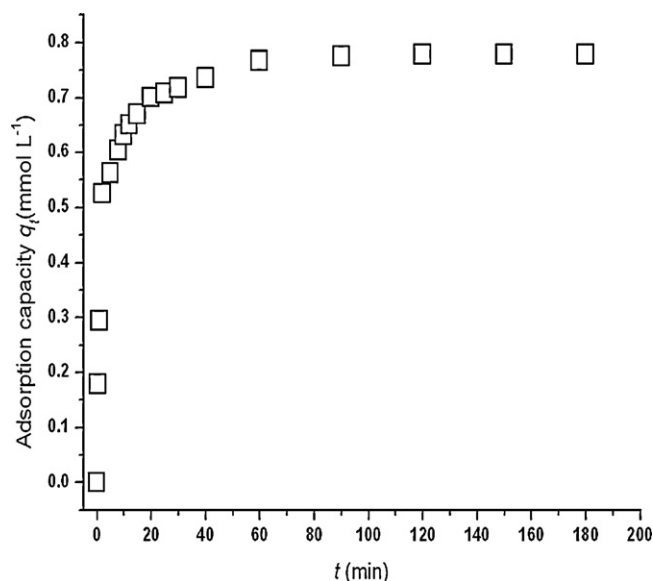

Fig. 6. Kinetics studies of Cr(III) adsorption onto BT–SiO$_2$ (pH 5.5, initial concentration of Cr(III) = 1.0 mmol L^{-1}).

The adsorption kinetic data were further analyzed using pseudo-first-order-rate model, which is expressed as [43]:

$$\log(q_e - q_t) = \log q_e - \frac{k}{2.303}t \tag{2}$$

where q_e and q_t are the amount of Cr(III) adsorbed (mmol L^{-1}) at equilibrium and at time t (min), respectively, and k is the rate constant of the pseudo-first-order-rate model (min^{-1}). Based on the experimental data of q_t and t, q_e, k, and the correlation coefficient (R^2) can be determined, respectively, from the slope and intercept of a plot of t/q_t versus t [44]. It was found that pseudo-first-order model gives a satisfied fitting to the experimental data with correlation coefficients higher than 0.99, and the calculated equilibrium adsorption capacity q_e is 0.76 mmol g^{-1}, which is very close to the experimentally determined adsorption capacity of 0.77 mmol L^{-1}. Consequently, the pseudo-first-order model can be used to describe the adsorption of Cr(III) onto BT–SiO$_2$ adsorbent.
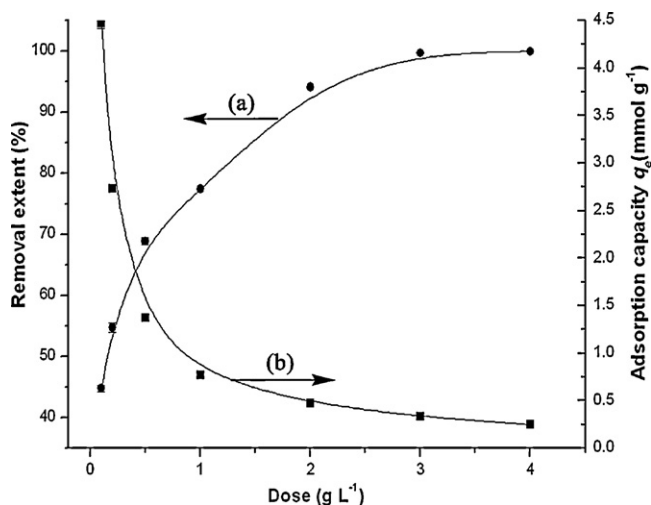

Fig. 7. Effect of adsorbent dose on the adsorption of BT–SiO$_2$ to Cr(III) (pH = 5.5, initial concentration of Cr(III) = 1.0 mmol L^{-1}).

Table 1
Effect of coexisting metal ions on the adsorption of BT–SiO$_2$ to Cr(III) (pH 5.5).

Adsorbent dose (g L^{-1})	Metal ions	Concentration before adsorption (mg L^{-1})	Concentration after adsorption (mg L^{-1})	Removal extent (%)
3.0	Cr(III)	52.14	0.82	98.44
	Fe(III)	5.52	0	100
	Cu(II)	6.58	0.17	97.49
	Al(III)	2.72	0.003	99.89
	Ca(II)	4.10	0.46	88.76
2.0	Cr(III)	52.14	3.85	92.62
	Fe(III)	5.52	0.19	96.58
	Cu(II)	6.58	0.58	91.19
	Al(III)	2.72	0.01	99.49
	Ca(II)	4.10	1.43	65.20
1.0	Cr(III)	52.14	9.85	81.12
	Fe(III)	5.52	1.07	80.66
	Cu(II)	6.58	1.96	70.28
	Al(III)	2.72	0.08	96.99
	Ca(II)	4.10	1.30	68.41

3.5. Effect of adsorbent dose on the adsorption of Cr(III)

As shown in Fig. 7(a), the removal extent of Cr(III) sharply increased with the increase of adsorbent dose in the range of 0.1–1.0 g L^{-1}, and then gradually reached the plateau in the range of 2.0–4.0 g L^{-1}. At lower dose, the adsorption sites of adsorbent are insufficient, resulting in a lower removal extent. On the other hand, the adsorption capacity of Cr(III) drastically decreased with the increasing adsorbent dose, as shown in Fig. 7(b). This is basically due to the fact that the adsorption sites of the adsorbent remain unsaturated at a fixed initial concentration of Cr(III) [45].

3.6. Effect of coexisting metal ions on the adsorption of Cr(III)

The effect of coexisting metal ions on the adsorption of BT–SiO$_2$ to Cr(III) are summarized in Table 1. It can be seen that the decrease of Cr(III) adsorption capacity was not remarkable and the removal extent of Cr(III) also increased with the increase of the adsorbent dose, indicating that coexisting metal ions had no obvious influence on the adsorption of BT–SiO$_2$ to Cr(III). Moreover, BT–SiO$_2$ showed strong adsorption abilities to the coexisting metal ions such as Al(III), Cu(II), Ca(II) and Fe(III). In fact, most of the metal ions coexisting in solutions were simultaneity removed when the adsorbent dose was 3.0 g L^{-1}. The possible explanation for this phenomenon could be that the adsorption capacity of BT–SiO$_2$ was large enough for adsorbing Cr(III) and other metal ions. Similar experimental results were also reported by other researchers [38]. These experimental results indicate that BT–SiO$_2$ can simultaneity remove Cr(III) and many other metal ions from aqueous solutions.

3.7. Stability of BT–SiO$_2$ adsorbent

In view of practical application, the BT immobilized onto SiO$_2$ beads should be stable during the adsorption process. Based on the Prussian Blue analysis method of tannin content, the concentration of BT leaked in Cr(III) solution after adsorption was found to be 3.65 mg L^{-1}, which indicates that the stability of BT–SiO$_2$ is satisfactory during adsorption process.

4. Conclusion

In this study, bayberry tannin-immobilized mesoporous silica bead (BT–SiO$_2$) had been successfully synthesized and applied for the removal of Cr(III) ions from aqueous solution. It was found that BT–SiO$_2$ had high adsorption capacity and fast adsorption rate for the removal of Cr(III). Further investigations revealed that the coex-

isting metal ions in solution had no influence on the adsorption of Cr(III) onto BT–SiO$_2$, and no bayberry tannin was leached out during the adsorption process. Therefore, mesoporous SiO$_2$ bead is an ideal matrix for the preparation of tannin-immobilized adsorbent, which can effectively remove heavy metals from aqueous solutions.

Appendix A. Supplementary data

Supplementary data associated with this article can be found, in the online version, at doi:10.1016/j.jhazmat.2009.08.003.

References

[1] D. Mohan, C.U. Pittman, Activated carbons and low cost adsorbents for remediation of tri- and hexavalent chromium from water, J. Hazard. Mater. 137 (2006) 762–811.
[2] D.E. Kimbrough, Y. Cohen, A.M. Winer, L. Creelman, C.A. Mabuni, Critical assessment of chromium in the environment, Crit. Rev. Environ. Sci. Technol. 29 (1999) 1–46.
[3] F. Gode, E. Pehlivan, Removal of chromium(III) from aqueous solutions using Lewatit S 100: the effect of pH, time, metal concentration and temperature, J. Hazard. Mater. 136 (2006) 330–337.
[4] D. Aderhold, C.J. Williams, R.G.J. Edyvean, The removal of heavy-metal ions by seaweeds and their derivatives, Bioresour. Technol. 58 (1996) 1–6.
[5] S.S. Madaeni, Y. Mansourpanah, COD removal from concentrated wastewater using membranes, Filtr. Separat. 40 (2003) 40–46.
[6] N. Kongsricharoern, C. Polprasert, Chromium removal by a bipolar electrochemical precipitation process, Water Sci. Technol. 34 (1996) 109–116.
[7] Y. Fernandez, E. Maranon, L. Castrillon, I. Vazquez, Removal of Cd and Zn from inorganic industrial waste leachate by ion exchange, J. Hazard. Mater. 126 (2005) 169–175.
[8] N. Ortiz, M.A.F. Pires, J.C. Bressiani, Use of steel converter slag as nickel adsorber to wastewater treatment, Waste Manage. 21 (2001) 631–635.
[9] Y. Xu, L. Axe, N. Yee, J.A. Dyer, Bidentate complexation modeling of heavy metal adsorption and competition on goethite, Environ. Sci. Technol. 46 (2006) 2213–2218.
[10] A. Lodi, D. Soletto, C. Solisio, A. Converti, Chromium(III) removal by *Spirulina platensis* biomass, Chem. Eng. J. 136 (2008) 151–155.
[11] J. Lach, E. Okoniewska, E. Neczaj, E.M. Kacprzak, The adsorption of Cr(III) and Cr(VI) on activated carbons in the presence of phenol, Desalination 223 (2008) 249–255.
[12] F. Gode, E. Pehlivan, Adsorption of Cr(III) ions by Turkish brown coals, Fuel Process. Technol. 86 (2005) 875–884.
[13] A. Demirbas, Heavy metal adsorption onto agro-based waste materials: a review, J. Hazard. Mater. 157 (2008) 220–229.

[14] B.H. Cruz, J.M. Diaz-Cruz, C. Arino, R. Tauler, M. Esteban, Multivariate curve resolution of polarographic data applied to the study of the copper-binding ability of tannic acid, Anal. Chim. Acta 424 (2000) 203–209.

[15] H.W. Ma, X.P. Liao, X. Liu, B. Shi, Recovery of platinum(IV) and palladium(II) by bayberry tannin immobilized collagen fiber membrane from water solution, J. Membr. Sci. 278 (2006) 373–380.

[16] M. Ozacar, I.A. Sengil, H. Turkmenler, Equilibrium and kinetic data, and adsorption mechanism for adsorption of lead onto valonia tannin resin, Chem. Eng. J. 143 (2008) 32–42.

[17] H. Yamguchi, R. Higasida, M. Higuchi, N. Sakata, Adsorption mechanism of heavy-metal ion by microspherical tannins resin, J. Appl. Polym. Sci. 45 (1992) 1463–1472.

[18] X.P. Liao, B. Shi, The collagen fiber immobilized tannins and their adsorption behaviors for heavy metal ions, in: Information: 6th Asian International Conference of Leather Science and Technology, 2004, pp. 181–191.

[19] A. Nakajima, T. Sakaguchi, Recovery of uranium by tannins immobilized on agarose, J. Chem. Technol. Biotechnol. 40 (1987) 223–232.

[20] L. Lima, S. Olivares, F. Martinez, J. Torres, D. de la Rosa, C. Septilveda, Use of immobilized tannin adsorbent for removal of Cr(VI) from water, J. Radioanal. Nucl. Chem. 231 (1998) 35–40.

[21] I. Chibata, T. Tosa, T. Mori, T. Watanabe, N. Sakata, Immobilized tannins—a novel adsorbent for protein and metal ion, Enzyme Microb. Technol. 8 (1986) 130–136.

[22] X. Huang, L.M. Jiao, X.P. Liao, B. Shi, Adsorptive removal of As(III) from aqueous solution by Zr(IV)-loaded collagen fiber, Ind. Eng. Chem. Res. 47 (2008) 5623–5628.

[23] X.P. Liao, W. Tang, R.Q. Zhou, B. Shi, Adsorption of metal anions of vanadium(V) and chromium(VI) on Zr(IV)-impregnated collagen fiber, Adsorption 14 (2008) 55–64.

[24] R. Wang, X.P. Liao, S.L. Zhao, B. Shi, Adsorption of bismuth(III) by bayberry tannin immobilized on collagen fiber, J. Chem. Technol. Biotechnol. 81 (2006) 1301–1306.

[25] O. Zaporozhets, N. Petruniock, O. Bessarabova, V. Sukhan, Determination of Cu(II) and Zn(II) using silica gel loaded with 1-(2-thiasolylazo)-2-naphthol, Talanta 49 (1999) 899–906.

[26] M. Naczk, F. Shahidi, Phenolics in cereals, fruits and vegetables: occurrence, extraction and analysis, J. Pharmaceut. Biomed. 41 (2006) 1523–1542.

[27] National stand method of china: GB 2615-81.

[28] F.L. Cheng, L.L. Chen, W. Wang, L.L. Liu, L. Deng, Immobilization and stabilization of papain on SiO$_2$ particles containing amine groups, Chin. J. Biotechnol. 20 (2004) 287–290 (in Chinese).

[29] M.L. Price, L.G. Butler, Rapid visual estimation and spectrophotometric determination of tannin content of sorghum grain, J. Agric. Food Chem. 25 (1977) 1268–1273.

[30] H. Aydin, Y. Bulut, C. Yerlikaya, Removal of copper (II) from aqueous solution by adsorption onto low-cost adsorbents, J. Environ. Manage. 87 (2008) 37–45.

[31] X.M. Zhan, X. Zhao, Mechanism of lead adsorption from aqueous solutions using an adsorbent synthesized from natural condensed tannin, Water Res. 37 (2003) 3905–3912.

[32] X.J. Chang, Z.H. Li, Y.M. Cui, X.B. Zhu, Z.P. Zang, Silica gel-immobilized-vanillin derivatives as selective solid-phase extractants for determination of chromium (III) in environmental samples by ICP-OES, Microchem. J. 90 (2008) 71–76.

[33] E. Robens, A. Dabrowski, V.V. Kutarov, Comments on surface structure analysis by water and nitrogen adsorption, J. Therm. Anal. Calorim. 76 (2004) 647–657.

[34] Y.S. Tao, H. Kanoh, K. Kaneko, Developments and structures of mesopores in alkaline-treated ZSM-5 zeolites, Adsorption 12 (2006) 309–316.

[35] E.P. Barrett, L.G. Joyner, P.H. Halenda, The determination of pore volume and area distributions in porous substances. I. Computations from nitrogen isotherms, J. Am. Chem. Soc. 73 (1951) 373–380.

[36] S.H. Joo, S. Jun, R. Ryoo, Synthesis of ordered mesoporous carbon molecular sieves CMK-1, Micropor. Mesopor. Mater. 44 (2001) 153–158.

[37] S.J. Han, K. Sohn, T. Hyeon, Fabrication of new nanoporous carbons through silica templates and their application to the adsorption of bulky dyes, Chem. Mater. 12 (2000) 3337–3341.

[38] Y. Wu, S.Z. Zhang, X.Y. Guo, H.L. Huang, Adsorption of chromium(III) on lignin, Bioresour. Technol. 99 (2008) 7709–7715.

[39] I. Langmuir, The constitution and fundamental properties of solids and liquids, J. Am. Chem. Soc. 38 (1916) 2221–2295.

[40] E.A. Oliveira, S.F. Montanher, A.D. Andrade, J.A. Nobrega, M.C. Rollemberg, Equilibrium studies for the sorption of chromium and nickel from aqueous solutions using raw rice bran, Process Biochem. 40 (2005) 3485–3490.

[41] M.F. Zhao, Z.B. Tang, P. Liu, Removal of methylene blue from aqueous solution with silica nano-sheets derived from vermiculite, J. Hazard. Mater. 158 (2008) 43–51.

[42] Z. Al-Qodah, W.K. Lafi, Z. Al-Anber, M. Al-Shannag, A. Harahsheh, Adsorption of methylene blue by acid and heat treated diatomaceous silica, Desalination 217 (2007) 212–224.

[43] M.S. Chiou, H.Y. Li, Adsorption behavior of reactive dye in aqueous solution on chemical cross-linked chitosan beads, Chemosphere 50 (2003) 1095–1105.

[44] M.C. Ncibi, B. Mahjoub, M. Seffen, Investigation of the sorption mechanisms of metal-complexed dye onto *Posidonia oceanica* (L.) fibres through kinetic modelling analysis, Bioresour. Technol. 99 (2008) 5582–5589.

[45] C. Raji, T.S. Anirudhan, Kinetics of Pb(II) adsorption by polyacrylamide grafted sawdust, Indian J. Chem. Technol. 4 (1997) 157–162.